A GCM Comparison of Plio-Pleistocene SuperInterglacial Periods in Relation to Lake El'gygytgyn, NE Arctic Russia

Anthony J. Coletti[1], Robert M. DeConto[1], Julie Brigham-Grette[1], Martin Melles[2]

[1] Department of Geosciences, University of Massachusetts, Amherst, MA, 01003, USA
[2] Institute of Geology and Mineralogy, University of Cologne, Zuelpicher Strasse 49a, D-50674 Cologne, Germany

Abstract

Until now, the lack of time-continuous, terrestrial paleoenvironmental data from the Pleistocene Arctic has made model simulations of past interglacials difficult to assess. Here, we compare climate simulations of four warm interglacials at Marine Isotope Stage (MIS) 1 (9ka), 5e (127 ka), 11c (409 ka), and 31 (1072 ka) with new proxy climate data recovered from Lake El'gygytgyn, NE Russia. Climate reconstructions of the Mean Temperature of the Warmest Month (MTWM) indicate conditions up to 0.4, 2.1, 0.5 and 3.1 ºC warmer than today during MIS-1, 5e, 11c, and 31, respectively. While the climate model captures much of the observed warming during each interglacial, largely in response to boreal summer (JJA) orbital forcing, the extraordinary warmth of MIS-11c relative to the other interglacials in the Lake El'gygytgyn temperature proxy reconstructions remains difficult to explain. To deconvolve the contribution of multiple influences on interglacial warming at Lake El'gygytgyn, we isolated the influence of vegetation, sea ice, and circum-Arctic land ice feedbacks on the modeled climate of the Beringian interior. Simulations accounting for climate-vegetation-land surface feedbacks during all four interglacials show expanding boreal forest cover with increasing summer insolation intensity. A deglaciated Greenland is shown to have a minimal effect on Northeast Asian temperature during the warmth of stage 11c and 31 (Melles et al., 2012). A prescribed enhancement of oceanic heat transport into the Arctic Ocean does have some effect

on Lake El'gygytgyn regional climate, but the exceptional warmth of MIS-l1c remains enigmatic relative to the modest orbital and greenhouse gas forcing during that interglacial.

1. Introduction

Knowledge of Pleistocene climate history has increased dramatically over the past three decades, however existing records remain strongly biased toward an oceanic viewpoint, due to the lack of long terrestrial archives. In the context of future warming, it is clearly important to understand the effects of warming on the terrestrial Arctic, the strength of polar amplification, and systemic teleconnections to and from other latitudes. Past warm periods known as Interglacials, over the past 2.8 million years, provide a means of studying climates warmer than today.

In 2009, a multinational team drilled a sediment core from a 25 km wide impact crater lake named Lake El'gygytgyn (alternatively, Lake "E"), in northeast Siberia (Brigham-Grette et al., 2013; Melles et al., 2012). The core contains the longest Arctic terrestrial record ever recovered, extending back ~3.5 million years, and provides evidence for periods of exceptional warmth during Pleistocene interglacials as defined by marine benthic $\delta^{18}O$ records (Lisiecki and Raymo, 2005) (Fig. 1A&B). It has been shown that Marine Isotope Stage(s) 1, 5e, 11c and 31 were among the warmest interglacials in the Pleistocene Arctic (Melles et al., 2012).

To explore the sensitivity of northwestern Beringia to interglacial forcing and the mechanisms responsible for the observed climate changes, we use a Global Climate Model coupled to an interactive vegetation model to simulate the terrestrial Arctic's response to the greenhouse gas and astronomical forcing associated with specific interglacial (e.g., Yin and Berger, 2011). A range of sensitivity tests were performed and changes in boundary conditions are imposed to test the response of the region to changes in circum-Arctic ice sheets and possible changes of ocean heat transport into the Arctic Ocean. In this text, we will outline changes in radiative forcing attributed to orbital changes while also outlining

changes in temperature, precipitation and vegetation in detail, assumed to also be related to these changes. The results are then compared to the Lake E multi-proxy reconstructions.

2. Model and experimental design

All global climate simulations discussed herein were performed using the current version of the Global ENvironmental and Ecological Simulation of Interactive Systems (GENESIS) Global Climate Model (GCM) version 3.0 (Alder et al., 2011; Thompson and Pollard, 1997). GENESIS is an atmosphere, land-surface, ocean, snow, sea ice, ice sheet and vegetation coupled model. As used here, spectral resolution of the atmosphere GCM is a T31 resolution (approximately 3.75° resolution) with 18 vertical levels (Thompson and Pollard, 1997). The AGCM is coupled to 2ºx2º soil, snow, vegetation, ocean, and sea ice model components. The GCM is interactively coupled to the BIOME4 (Kaplan, 2003) vegetation model that predicts equilibrium vegetation distribution, structure and biogeochemistry using monthly mean climatologies of precipitation, temperature and clouds simulated by the GCM. Vegetation distributions take the form of 27 plant biomes including 12 plant functional types (PFTs) that represent broad, physiologically distinct classes (Kaplan, 2003). GENESIS includes options for coupling to an Ocean General Circulation Model (Alder et al., 2011) or a non-dynamical, slab ocean model that incorporates heat transfer, calculations of sea-surface temperatures (SST) and feedbacks operating between ocean surface and sea ice. The slab mixed layer ocean model is used here to allow multiple simulations to be performed with and without imposed perturbations of surface ocean conditions. This version of the GCM has a sensitivity of 2.9 °C, without GHG, vegetation or ice sheet feedbacks. Greenhouse gases and orbital parameters for each interglacial simulation were prescribed according to ice core records (Loulergue et al., 2008; Lüthi et al., 2008; Schilt et al., 2010) and standard astronomical solutions (Berger, 1978).

The strategy adopted here was to target Marine Isotope Stage (MIS) 1 (11 ka), 5e (127 ka), 11c (409 ka) and 31 (1072 ka), corresponding to the timing of peak summer (July) warmth observed at Lake E and identified as “super-interglacials” by Melles et al., (2012). Equilibrium simulations were performed at the time of peak boreal summer insolation at

67.5°N (Berger, 1978) assuming the real climate system equilibrated within a half-precession cycle. Model temperature and precipitation values were calculated from 20-year averages taken from the 60 to 80-year equilibrated simulations. Preliminary analysis of pollen assemblages in the Lake E core is assumed to provide a record of peak summer temperatures, so our data-model comparisons focus on warmest monthly mean climate (July). A simulation of preindustrial climate (280 ppmv pCO_2) was run as a control experiment to evaluate the model's representation of Beringian climate and to provide a baseline for comparing super-interglacial simulations. A modern Greenland Ice Sheet (GIS) is prescribed unless otherwise noted. In simulations without a GIS, the ice sheet is replaced with ice-free, isostatically equilibrated land surface elevations.

2.1 MIS 1, 9 ka

MIS-1 represents the last 11,000 years and its onset roughly coincides with the end of the Younger-Dryas (~11,500 ka). Peak boreal summer insolation occurs ~9 ka, when summer insolation was ~510 Wm^{-2} at 65 °N, relative to 446 Wm^{-2} today. Proxy indicators suggest conditions were warmer than present (+1.6 °C over western Arctic and +2 to 4°C in circum-Arctic) with lush birch and alder shrubs (Melles et al., 2012) dominating the vegetation around the lake. This period, known as the Holocene Climate Optimum (HCO), was spatially variable, with most warming in the high latitudes, and minimal warming in the mid-latitudes and tropics (Kitoh and Murakami, 2002).

2.2 MIS-5e, 127 ka

MIS-5e, also known as the Last Interglaciation (LIG), is one of the warmest interglacials of the Pleistocene and lasted roughly ~14 kyr (130 to 116 ka). High obliquity, eccentricity and the timing of perihelion (precession) combined to produce high intensity boreal summer insolation at around 127 ka. Greenland ice core records (Dahl-Jensen and NEEM community members, 2013) suggest summer warming up to 8±4 ºC over northeast Greenland, but only a modest reduction in the size of the Greenland Ice Sheet (GIS). Studies involving Sr – Nd – Pb isotope ratios of silt-sized sediment discharged from southern Greenland suggest that no single southern Greenland geologic terrain was

completely deglaciated during the LIG, however, some southern GIS retreat was evident (Colville et al., 2011). A previous model study of MIS-5e by (Yin and Berger, 2011) involved running a model of intermediate complexity to test relative contributions of Greenhouse Gas (GHG) and insolation forcing on LIG warmth. They found that GHGs play a dominant role on the variations of the annual mean temperature of both the globe and the southern high latitudes, whereas, insolation plays a dominant role on precipitation, northern high latitude temperatures, and sea ice extent (Yin and Berger, 2011). Similarly, model simulations have shown that insolation anomalies during MIS-5e likely caused significant summer (JJA) warming throughout the Arctic (Bakker et al., 2013; Lunt et al., 2013; Otto-Bliesner et al., 2006).

The LIG simulation shown here is used to compare paleoenvironmental conditions in western Beringia, including, temperature, vegetation and precipitation, to Lake E pollen proxy analysis. Orbital parameters and greenhouse gas concentrations are set at their 127 ka values to represent peak boreal warmth during MIS-5e.

2.3 MIS-11c, 409 kyr

MIS-11c is another exceptionally warm interglacial (Howard, 1997) that lasted from 428 to 383 ka (~45 ka). Sediment records from the Arctic containing information on MIS-11 are generally lacking (Miller et al., 2010b). Unlike the other interglacials, MIS-11c was remarkably long, with two boreal insolation maxima at ~409 ka and 423 ka, creating extensive warmth throughout the Arctic (Melles et al., 2012). Unlike MIS-5e, there is evidence that the GIS may have been reduced in size (Raymo and Mitrovica, 2012; Willerslev et al., 2007), with lush boreal forest covering most of southern Greenland (de Vernal and Hillaire-Marcel, 2008). Particularly warm conditions are also suggested by pollen records analyzed from Lake Biwa (Tarasov et al., 2011) located in Shiga Prefecture, Japan. Likewise, a study from Lake Baikal also indicates warmer than modern temperatures with a “conifer optimum” suggesting warmer conditions and less aridity, perhaps influenced by higher sea levels and reduced continentality (Prokopenko et al., 2010).

Three different simulations (Table 1, 2) were run to test the sensitivity of the lake region to MIS-11c forcing. The first simulation uses default boundary conditions, including a modern GIS (MIS11GIS). The second simulation tests the sensitivity of the Lake E region to an ice-free Greenland (MIS11NG). In this simulation, the entire GIS was removed and replaced with bare soil, and the topography of Greenland was corrected for glacial isostatic adjustment. The final sensitivity experiment includes an increase in sub-sea ice surface heat flux from 2 Wm^{-2} in our preindustrial control, to 10 Wm^{-2} (additional +8 Wm^{-2}) to test the Beringian sensitivity to a mostly ice-free Arctic Ocean. The increased heat flux assumes an extreme ~3 Sverdrup (Sv) increase in Bering Strait through flow and a 4 °C temperature contrast between North Pacific and North Polar surface water (Melles et al., 2012, supplemental). The additional heat flux convergence is used to crudely mimic the influence of a wider and deeper Bering Strait during times of higher sea level. Using the predictive BIOME4 interactive vegetation model, direct comparisons of observed and modeled Arctic vegetation within the Lake E region can be made. Furthermore, simulations using prescribed distributions of biome flora can be used to quantify the local effect of changing vegetation cover around the region.

2.4 MIS-31, 1072 ka

MIS-31 (~1062-1082 ka) (Lisiecki and Raymo, 2005) has only been identified in a few Arctic records prior to Lake E. The Interglacial represents one of the last 41-kyr glacial cycles and is best known for extreme warmth in circum-Antarctica ocean waters induced by a deterioration of the Polar Front (Scherer et al., 2008) and the collapse of the marine based West Antarctic Ice Sheet (WAIS) (DeConto et al., 2012; Pollard & DeConto, 2009), by intrusion of warm surface waters onto Antarctic continental shelves. On Ellesmere Island, Fosheim Dome includes terrestrial deposits that date to ~1.1 Ma, which contains fossil beetle assemblages dated within MIS-31, suggesting temperatures of 8 to 14 °C above modern values (Elias and Matthews Jr., 2002). It is speculated, like MIS-11c, that the Arctic may have been too warm to support a GIS which may have been substantially reduced in size, or possibly nonexistent (Melles et al., 2012; Raymo and Mitrovica, 2012). Therefore, simulations of MIS-31 are run both with and without a GIS (Table 1, 2).

3. Results

3.1 Control Simulation

3.1.1 Preindustrial

Simulations of preindustrial 2-m mean annual temperature (MAAT) and MTWM (July) at Lake E are -12 and 10.3 °C respectively. Preindustrial summer temperatures (8 °C) are -2.2 °C lower than modern. GHG radiative forcing from a combination of CO_2, CH_4, and N_2O atmospheric mixing ratios implies a 1.8 Wm^{-2} reduction relative to modern, accounting for most of the cooling in the preindustrial simulation. Generally, mean annual precipitation (PANN) values in the cooler, preindustrial simulation are slightly lower than modern precipitation. At Lake E, preindustrial annual precipitation was 438 mm $year^{-1}$. Winter (DJF) precipitation in the preindustrial simulation was ~24 mm $month^{-1}$, while mean summer (JJA) precipitation was 43 mm $month^{-1}$.

Simulated preindustrial vegetation distributions are assumed to be in equilibrium (Fig. 2A). In the preindustrial simulation, shrub tundra dominates the Lake E region, with evergreen taiga and deciduous forests maintained in interior Siberia and Yukon. Simulated Siberian biome distributions are similar to modern day vegetation described by Kolosova (1980) and Viereck & Little Jr (1975). Shrub tundra in the preindustrial simulation can be attributed to cool and dry Arctic conditions in the preindustrial run.

3.2 Paleoclimate simulations

3.2.1 MIS-1 (9 ka); Holocene Thermal Maximum

July temperatures at Lake E in the MIS-1 simulation (12.4 °C) are ~2.1 °C warmer than preindustrial (10.3 °C) and summer (JJA) temperatures are 1.6 °C warmer (Fig. 3A). Overall, the Siberian interior warms > 5 °C in July, relative to preindustrial. Simulated MTWM exceed > 2 °C around Lake E.

Simulated MIS-1 PANN values at the lake (~438 mm $year^{-1}$) are close to preindustrial values, although somewhat drier conditions dominate further inland, possibly a result attributed to increased proximity away from a moisture source. Simulated

vegetation around Lake E is close to the transition between dominant shrub tundra to the east and deciduous forest to the west (Fig. 2B).

3.2.2 MIS-5e (127 ka)

Overall warming of the Beringian interior in the MIS-5e simulation is > 2 °C relative to preindustrial temperatures (Fig. 3B). Most of this warming can be attributed to the direct effects of the MIS-5e orbit (Groll et al., 2005; Langebroek and Nisancioglu, 2014), which produces an Arctic summer insolation anomaly of >50 Wm^{-2} at the top of the atmosphere, relative to a preindustrial (modern) orbit (Fig. 4B). According to ice core records, carbon dioxide (CO_2) concentrations during this period were about 287 ppmv (Hönisch et al., 2009), contributing 0.132 Wm^{-2} more surface radiative forcing than preindustrial, but the combination of CO_2, CH_4, and N_2O attributes 0.0035 Wm^{-2} less forcing relative to preindustrial GHG mixing ratios.

Comparing MIS-5e with respect to the preindustrial control simulation at Lake E shows differences in summer (JJA) and MTWM temperatures of +2.5 and +4.2 °C, respectively (Fig. 3B). Summer warming over the GIS is +5 °C relative to preindustrial, which is comparable to the LIG warming reported in a recent Greenland ice core study (Dahl-Jensen and NEEM community members, 2013). Mean annual precipitation at Lake E (~401 mm $year^{-1}$), is 37 mm $year^{-1}$ less than preindustrial levels, and the difference is statistically significant at the 95% confidence level with a p-value of 0.029. Overall, similar precipitation patterns are seen at Lake E, relative to MIS-5e and the preindustrial control scenario, which reflects both the overall wet bias in the GCM and the similar continental/ice sheet boundary conditions, in both simulations.

A less moist, but warm high latitude environment produces deciduous taiga and evergreen taiga biome distributions around Lake E (Fig. 2C), with evergreen taiga being the most dominant in eastern Beringia and deciduous taiga being more dominant around the Lake E region and most of western Beringia.

3.2.3 MIS-11c (409 ka)

Due to an eccentricity minimum, MIS-11c is a longer interglacial than the other interglacials in this study (Howard, 1997). We assume an ice-free Greenland in our MIS-11c simulations, with the ice sheet removed and replaced with isostatically equilibrated (ice-free) land elevations. Additional experiments including an imposed increase in sub-sea ice heat flux in the Arctic Ocean basin will also be discussed.

Model simulations show summer insolation anomalies (relative to preindustrial) during MIS-11c ranging from +45 – 55 Wm^{-2} (Fig. 4C) allowing temperatures over the Lake E region during July (month of maximum insolation) to increase 2.2 °C relative to preindustrial. Overall, mean annual summer temperatures (JJA) over the circum-Arctic and Lake E are 2 to 4 °C warmer than preindustrial temperatures, with the Siberian interior warming the most (Table 2).

In MIS-11c simulations performed with (MIS11GIS) and without a GIS (MIS11NG), the effect on temperature at the Lake E is shown to be small (~0.3 °C). Geopotential height anomalies at 500hPa (+4 – 10 meters) indicate upper-level warming east of Lake E, and cooling west of Lake E, but the net effect of ice sheet loss on surface air temperatures is mostly limited to Greenland itself and the proximal ocean, with little effect at the distance of Lake E, as shown in other modeling studies (Koenig et al., 2012; Otto-Bliesner et al., 2006).

The warm MIS-11c climate and possible reductions of Greenland and West Antarctic ice sheet sheets are thought to have contributed to sea levels as much as >11 meters (Raymo and Mitrovica, 2012) higher than today. Arctic sea ice was also possibly reduced (Cronin et al., 2013; Polyak et al., 2010). In order to test the influence of high sea levels and a mostly ice-free Arctic Ocean on Lake E climate, heat flux convergence under sea ice was increased from 2 Wm^{-2} to 10 Wm^{-2} in the slab ocean/dynamic sea ice model. The resulting reductions in sea ice extent and warmer (~ 0.2 – 1.0 °C) (Fig. 5A) Arctic SST's produced negligible warming around Lake E (< 0.7 °C), suggesting the Lake E region was relatively insensitive to Arctic Ocean conditions.

Precipitation amounts at Lake E during MIS11GIS are greater than preindustrial values (438 mm $year^{-1}$). Also, MIS11NG exhibits the same precipitation amounts as our preindustrial control run (~438 mm $year^{-1}$) (Table 2). Simulated precipitation conditions in the Arctic Ocean basin are fairly dry, ~200 mm $year^{-1}$, comparable to reanalysis data sets

(Serreze and Hurst, 2000). On the contrary, simulations of MIS11NG show reduced precipitation amounts by -37 mm $year^{-1}$ relative to MIS11GIS. Runs with increased sub-ice oceanic heat flux reduced the drying seen in the MIS11NG simulation and produced values greater than the preindustrial control (~475 mm $year^{-1}$).

A warmer and wetter MIS-11c places Lake E on the border of evergreen taiga and shrub tundra biomes (Fig. 2D). Vegetation limits, such as tree lines, are slightly changed during our simulations with increased heat flux and a warmer, open Arctic Ocean. Evergreen forests around the Lake E region extend poleward to the coast and slightly eastward.

3.2.4 MIS-31 (1072 ka)

A warm orbit with high obliquity, high eccentricity and precession aligning perihelion with boreal summer allows insolation anomalies to be > 50 Wm^{-2} at the surface and + 60 – 80 W m^{-2} (Fig. 4D) at the top of the atmosphere at the latitude of Lake E. Average summer (JJA) temperatures around the lake are about +3.8 °C warmer than preindustrial (Fig. 3D; Table 2). While MIS-31 is beyond the temporal range of ice core greenhouse gas records, proxy geochemical records imply MIS-31 has the highest pCO_2 (~325 ppmv) of the mid-Pleistocene (Hönisch et al., 2009), contributing ~+0.80 Wm^{-2} relative to preindustrial values. As a result, modeled July temperatures at Lake E are >5 °C warmer than preindustrial temperatures.

Simulated precipitation at Lake E during MIS-31 is ~438 mm $year^{-1}$ (Table 2), similar to that in MIS-11c simulations. Vegetation distribution is similar to the other interglacials described here (Fig. 2E). The Lake E region is dominated by evergreen taiga.

4. Discussion

The warm periods of Marine Isotope Stage(s) 1, 5e, 11c and 31 show similar changes around Lake E. Temperature reconstructions during the Holocene Thermal Maximum (9 kyr) indicate +1.6 (±0.8) °C warming in the western Arctic (Kaufman and Brigham-Grette, 1993) with an overall warming of 1.7 (±0.8) °C in the circum-Arctic

(Miller et al., 2010a), relative to modern temperatures. Though our model does not fully account for all the warming during this period, it does produce the warming in the western Arctic as documented by Kaufman and Brigham-Grette (1993). With the decrease in Arctic moisture and low CO_2, deciduous and evergreen forests dominate the Arctic in the model, matching the dominant vegetation such as *Alnus, Betula* (nut bearing trees and fruits), *Poaceae* (grasses) and some birch and alder seen in the Lake E record (Melles et al., 2012).

Marine Isotope Stage 5e produced the greatest summer warming among the four interglacials simulated here. Comparisons with a preindustrial control run show that differences in MTWM at Lake E during MIS-1 and 5e (+2.1 and +4.2 °C) are similar to the changes seen in MIS11NG and MIS-31(+2.2 and +3.5 °C) (Table 2). Similar warming has been seen in other modeling studies showing that a high obliquity and high eccentricity with precession aligning perihelion with boreal summer will yield the warmest boreal summer temperatures (Koenig et al., 2011; Lunt et al., 2013; Otto-Bliesner et al., 2006; Yin and Berger, 2011). Strong insolation forcing at these latitudes cause July maximum temperatures to exceed preindustrial temperatures by >2 °C. The 2–4 °C simulated MIS-5e warming in Siberia and Lake E has also been seen in proxy data compilations (CAPE, 2006; Lozhkin and Anderson (1995); Lozhkin et al. (2006)) and in simulations using a GCM without vegetation feedbacks (Otto-Bliesner et al., 2006). Most of the warming has been linked to the summer insolation anomaly associated with the MIS-5e orbit (Otto-Bliesner et al., 2006). The exceptional summer warmth of MIS-5e compared to other interglacials was previously thought to have caused a substantial reduction in the GIS, however, more recent work suggests the GIS contributed only ~1.4 to 4.3 m of equivalent eustatic sea level rise during the LIG (Colville et al., 2011; Quiquet et al., 2013; Robinson et al., 2011; Stocker et al., 2013; Stone et al., 2013), and remained mostly intact (Dahl-Jensen and NEEM community members, 2013). This suggests that our simulations of MIS-5e with a modern GIS are a good approximation for this period. Colder and fresher sea surface conditions in the North Atlantic, Labrador and Norwegian Seas have been found in marine sediments records possibly indicating freshwater input (perhaps from parts of Greenland) which may have led to early LIG warming attributed to stronger ocean overturning (Govin et al., 2012). In the model, Arctic warming during MIS-5e allows almost a full replacement of shrub tundra with deciduous forest in and around the Lake E

region. Pollen analysis during this period shows tree species of birch, alder, pine and spruce (Melles et al., 2012). However, multiproxy studies of MIS-5e show a change in MTWM of only +2 °C compared to modern temperatures (Melles et al., 2012) (Table 2). It can be concluded that the warm boreal summer orbit at MIS-5e can account for much of the warmth in Beringia, and the cirum-Arctic, but the particularly muted response in the Lake E proxy record to summer insolation forcing cannot be fully explained.

Simulations of MIS-11c exhibit another very warm interglacial at Lake E, with MTWM maxima approaching +2.2 °C warmer than preindustrial temperatures (Table 2). Similarly to MIS-5e and 1, peak warmth coincides with perihelion during boreal summer, however low eccentricity and obliquity attenuates the effects of precession relative to 5e and 1, making summer insolation less intense. A combination of eccentricity, obliquity and precession elevates summer insolation for ~45k years, a much longer (but less intense) interval of elevated summer insolation than during the other interglacials studied here. The overall warmth of MIS-11 is, in part, an outcome of reduced snow and ice cover.

Another possible mechanism contributing to Lake E warmth at MIS-11 might be related to elevated sea level at this time (Raymo and Mitrovica, 2012), possibly contributing to increased Bering Strait through flow. Today, the Bering Strait is limited to ~50 m in depth with a net northward transport of ~0.8 Sv (Woodgate et al., 2010). Oceanic heat transport into the Arctic basin might have been elevated during high sea level, providing a source of warm water intrusion into the Arctic Ocean basin from the North Pacific. As a simple test of the potential for a warmer Arctic Ocean with less sea ice to affect temperatures over terrestrial Beringia, heat flux convergence under sea ice in the Arctic Ocean was increased from 2 to 10 W m^{-2}. Summer sea ice fraction was reduced by 25 – 50 % and summer ocean temperatures warmed by 0.2 – 1.0 °C (Fig. 5A,B). The simulated warming of the Arctic Ocean warmed the Lake E region, but only slightly (+0.7 °C), and does not account for the exceptional warmth observed during MIS-11c relative to MIS-5e.

The influence of MIS-11c temperatures on terrestrial biome distributions is supported in model simulations by a poleward advance of evergreen needle-leaf forest around the lake, which is in good agreement with palynological analysis (Melles et al., 2012) showing forest-tundra and northern larch-taiga dominated by spruce, pine, birch,

alder and larch (Melles et al., 2012). Surface warming as a result of albedo feedbacks associated with needle-leaf forests during snow-covered months accounts for some of the warming during this period, however increased evergreen, terrestrial forest and enhanced evapotranspiration provides a slight net cooling during the summers.

A deglaciated Greenland has been shown to have regional effects on SSTs and sea-ice conditions, however warming of the circum-Arctic has been shown to be minimal (Koenig et al., 2012; Otto-Bliesner et al., 2006). This is also demonstrated in our simulations, whereby the loss of the GIS warms summer annual temperatures around Lake E by only 0.3 °C (Table 2). An analysis of 500 hPa geopotential height anomalies show ridging (positive height anomalies of > 10 m) to the east and troughing (negative height anomalies) to the west of Lake E, indicating a slight change in the large-scale planetary wave patterns over Beringia. Over Lake E, positive height anomalies are also present, indicating slightly warmer conditions and a slight eastward shift of an atmospheric ridge that may have been set up further west of Lake E. The ridging in these simulations may also be related to a decrease in precipitation at Lake E when the GIS is removed in GCM. Extended high pressure over Beringia associated with ridging would create somewhat drier conditions for the region. If the exceptional warmth of MIS-11c is indeed related to the melting of the GIS, freshwater input may have been a mechanism to strengthen North Atlantic overturning creating the warmth missing in our simulations (Govin et al., 2012). Furthermore, it is not clear why the GIS would have survived MIS-5e warmth, and not MIS-11c. In sum, the exceptional Arctic warmth of MIS-11c remains difficult to explain and is not a straightforward result of greenhouse gases, orbital forcing, vegetation feedbacks, or Arctic Ocean warming.

Elevated GHG concentrations and a very warm summer orbit can explain much of the warmth during MIS-31, assuming atmospheric CO_2 was higher than MIS-5e and MIS-11 (Hönisch et al., 2009). In the model, the combination of elevated greenhouse gases and strong summer insolation forcing at 1072 ka allow dense needle-leaf and deciduous forests to grow around the Lake. Simulated summer temperatures are about 12 °C (Table 2), +2 °C warmer than modern summer temperatures around Lake E. Biome reconstructions derived from pollen analysis of the Lake E core (Melles et al., 2012) show a maxima of trees and shrubs during peak northern hemisphere insolation of MIS-31 at 1072 ka. Our

model simulations show similar results around Lake E, with increased boreal forest and less tundra and small dwarf shrubs. The snow-albedo effect combined with low-albedo forest cover allows temperatures to increase in the Arctic during MIS-31. Peak precipitation rates derived from proxy analysis indicate about 600 mm $year^{-1}$, or about 162 mm $year^{-1}$ more precipitation than in our preindustrial model simulation (Melles et al., 2012). GCM results at MIS-31 indicate annual precipitation of ~490 mm $year^{-1}$ (Table 2), the most annual precipitation among the four interglacials simulated here. While the GCM does not fully capture the enhanced precipitation indicated in the proxy record, a relative increase in precipitation is evident. Extraordinary warmth during MIS-31 correlates well with a diminished WAIS (Pollard and DeConto, 2009) implying strong inter-hemispheric coupling that has been related to possible reductions in Antarctic Bottom Water (AABW) formation during times of ice-shelf retreat and increased fresh water input into the Southern Ocean (Foldvik, 2004). WAIS collapse could also be linked with the Beringian and Lake E warmth during MIS-11c and MIS-5e, but definitive evidence of WAIS retreat during these later Pleistocene interglacials is currently lacking (McKay et al., 2012).

5. Conclusions

Lake E provides a high-resolution terrestrial proxy record of climate variability in the Arctic. A linked climate modeling study described here shows that Arctic summers were significantly warmer during several Pleistocene interglacials by as much as + 2 °C during MIS-1 and 11c, and by as much as + 4 °C during MIS-5e and 31 relative to preindustrial. It can be inferred that most of the warming in the interglacial simulations can be attributed to a combination of elevated GHGs and astronomical forcing, although, astronomical forcing (at times producing high-intensity summer insolation >50 Wm^{-2} higher than today) was the dominant warming mechanism. Greenhouse gas levels during MIS-31 remain poorly known, and the extreme warmth of this particular interglacial could have been substantially augmented by GHG forcing. MIS-1 had relatively low CO_2 around the time of peak Holocene warmth, producing 0.44 Wm^{-2} less radiative forcing relative to preindustrial levels (Melles et al., 2012), but the combination of orbital forcing and perhaps other factors such as changes in Antarctic Bottom Water (AABW) production and reduced

Arctic sea-ice may have contributed to exceptional Arctic warmth at this time. Thorough testing of these ideas will require additional simulations with coupled atmosphere-ocean models, changes in circum-arctic ice sheets, eustatic sea-levels, continentality, changes in sea-ice distributions and the addition of melt-water inputs into northern and southern hemisphere oceans.

Extreme interglacial warmth shifted Lake E vegetation from mostly tundra with small shrubs as we see the Arctic today to thick, lush evergreen and boreal forest. Due to the extreme warmth, wetter conditions prevailed during the super-interglacials, allowing forest biomes to thrive and increase their maximum extent poleward. While simulated warming at Lake E is broadly similar during each interglacial, the vegetation response in each simulation is unique, reflecting differences in seasonal temperatures and hydroclimate. The simulated absence of a Greenland Ice Sheet allowed summer temperatures to increase to almost 16 °C warmer than present over Greenland, but with limited impact on temperatures around Lake E. The observed response of Beringia's climate and terrestrial vegetation to super-interglacial forcing is still not fully understood and creates a challenge for climate modeling and for quantifying the strength of Arctic amplification. Among the interglacials studied here, MIS-11c is the warmest interglacial in the Lake E record, yet MIS-5e is the warmest simulated by the model. The model produces overall drier conditions in the earlier interglacials (11c and 31) than suggested by pollen analysis. If the proxy interpretations were correct, this would suggest that the model is missing some important regional processes. The timing of significant warming in the circum-Arctic can be linked to major deglaciation events in Antarctica, demonstrating possible inter-hemispheric linkages between the Arctic and Antarctic climate on glacial-interglacial timescales, which have yet to be explained.

References

Alder, J. R., Hostetler, S. W., Pollard, D. and Schmittner, A.: Evaluation of a present-day climate simulation with a new coupled atmosphere-ocean model GENMOM, Geosci. Model Dev., 4(1), 69–83, doi:10.5194/gmd-4-69-2011, 2011.

Bakker, P., Stone, E. J., Charbit, S., Gröger, M., Krebs-Kanzow, U., Ritz, S. P., Varma, V., Khon, V., Lunt, D. J., Mikolajewicz, U., Prange, M., Renssen, H., Schneider, B. and Schulz, M.: Last interglacial temperature evolution - a model inter-comparison, Clim. Past, 9(2), 605–619, doi:10.5194/cp-9-605-2013, 2013.

Berger, A.: Long-Term Variations of Daily Insolation and Quaternary Climatic Changes, J. Atmospheric Sci., 35(12), 2362–2367, doi:10.1175/1520-0469(1978)035<2362:LTVODI>2.0.CO;2, 1978.

Brigham-Grette, J., Melles, M., Minyuk, P., Andreev, A., Tarasov, P., DeConto, R., Koenig, S., Nowaczyk, N., Wennrich, V., Rosen, P., Haltia, E., Cook, T., Gebhardt, C., Meyer-Jacob, C., Snyder, J. and Herzschuh, U.: Pliocene Warmth, Polar Amplification, and Stepped Pleistocene Cooling Recorded in NE Arctic Russia, Science, 340(6139), 1421–1427, doi:10.1126/science.1233137, 2013.

Colville, E. J., Carlson, A. E., Beard, B. L., Hatfield, R. G., Stoner, J. S., Reyes, A. V. and Ullman, D. J.: Sr-Nd-Pb Isotope Evidence for Ice-Sheet Presence on Southern Greenland During the Last Interglacial, Science, 333(6042), 620–623, doi:10.1126/science.1204673, 2011.

Cronin, T. M., Polyak, L., Reed, D., Kandiano, E. S., Marzen, R. E. and Council, E. A.: A 600-ka Arctic sea-ice record from Mendeleev Ridge based on ostracodes, Sea Ice Paleoclimate Syst. Chall. Reconstr. Sea Ice Proxies, 79(0), 157–167, doi:10.1016/j.quascirev.2012.12.010, 2013.

Dahl-Jensen, D. and NEEM community members: Eemian interglacial reconstructed from a Greenland folded ice core, Nature, 493(7433), 489–494, doi:10.1038/nature11789, 2013.

DeConto, R. M., Galeotti, S., Pagani, M., Tracy, D., Schaefer, K., Zhang, T., Pollard, D. and Beerling, D. J.: Past extreme warming events linked to massive carbon release from thawing permafrost, Nature, 484(7392), 87–91, doi:10.1038/nature10929, 2012.

Elias, S. A. and Matthews Jr., J. V.: Arctic North American seasonal temperatures from the latest Miocene to the Early Pleistocene, based on mutual climatic range analysis of fossil beetle assemblages, Can. J. Earth Sci., 39(6), 911–920, doi:10.1139/e01-096, 2002.

Foldvik, A.: Ice shelf water overflow and bottom water formation in the southern Weddell Sea, J. Geophys. Res., 109(C2), doi:10.1029/2003JC002008, 2004.

Govin, A., Braconnot, P., Capron, E., Cortijo, E., Duplessy, J.-C., Jansen, E., Labeyrie, L., Landais, A., Marti, O., Michel, E., Mosquet, E., Risebrobakken, B., Swingedouw, D. and Waelbroeck, C.: Persistent influence of ice sheet melting on high northern latitude climate during the early Last Interglacial, Clim. Past, 8(2), 483–507, doi:10.5194/cp-8-483-2012, 2012.

Groll, N., Widmann, M., Jones, J. M., Kaspar, F. and Lorenz, S. J.: Simulated relationships between regional temperatures and large-scale circulation: 125 kyr BP (Eemian) and the preindustrial period, J. Clim., 18(19), 4032–4045, 2005.

Hönisch, B., Hemming, N. G., Archer, D., Siddall, M. and McManus, J. F.: Atmospheric Carbon Dioxide Concentration Across the Mid-Pleistocene Transition, Science, 324(5934), 1551–1554, doi:10.1126/science.1171477, 2009.

Howard, W. R.: Palaeoclimatology: A warm future in the past, Nature, 388(6641), 418–419, 1997.

Kaplan, J. O.: Climate change and Arctic ecosystems: 2. Modeling, paleodata-model comparisons, and future projections, J. Geophys. Res., 108(D19), doi:10.1029/2002JD002559, 2003.

Kaufman, D. S. and Brigham-Grette, J.: Aminostratigraphic correlations and paleotemperature implications, Pliocene-Pleistocene high-sea-level deposits, northwestern Alaska, Quat. Sci. Rev., 12(1), 21–33, doi:10.1016/0277-3791(93)90046-O, 1993.

Kitoh, A. and Murakami, S.: Tropical Pacific climate at the mid-Holocene and the Last Glacial Maximum simulated by a coupled ocean-atmosphere general circulation model, Paleoceanography, 17(3), 19–1–19–13, doi:10.1029/2001PA000724, 2002.

Koenig, S. J., DeConto, R. M. and Pollard, D.: Late Pliocene to Pleistocene sensitivity of the Greenland Ice Sheet in response to external forcing and internal feedbacks, Clim. Dyn., 37(5-6), 1247–1268, doi:10.1007/s00382-011-1050-0, 2011.

Koenig, S. J., DeConto, R. M. and Pollard, D.: Pliocene Model Intercomparison Project Experiment 1: implementation strategy and mid-Pliocene global climatology using GENESIS v3.0 GCM, Geosci. Model Dev., 5(1), 73–85, doi:10.5194/gmd-5-73-2012, 2012.

Kolosova, L.: Geographical Atlas, 1980.

Langebroek, P. M. and Nisancioglu, K. H.: Simulating last interglacial climate with NorESM: role of insolation and greenhouse gases in the timing of peak warmth, Clim. Past, 10(4), 1305–1318, doi:10.5194/cp-10-1305-2014, 2014.

Lisiecki, L. E. and Raymo, M. E.: A Pliocene-Pleistocene stack of 57 globally distributed benthic δ18O records, Paleoceanography, 20(1), PA1003, doi:10.1029/2004PA001071, 2005.

Loulergue, L., Schilt, A., Spahni, R., Masson-Delmotte, V., Blunier, T., Lemieux, B., Barnola, J.-M., Raynaud, D., Stocker, T. F. and Chappellaz, J.: Orbital and millennial-scale features of atmospheric CH4 over the past 800,000 years, Nature, 453(7193), 383–386, doi:10.1038/nature06950, 2008.

Lozhkin, A. V. and Anderson, P. M.: The Last Interglaciation in Northeast Siberia, Quaternary Research, 43, 147–158, 1995.

Lozhkin, A. V., Anderson, P. M., Matrosova, T. V. and Minyuk, P. S.: The pollen record from El'gygytgyn Lake: implications for vegetation and climate histories of northern Chukotka since the late middle Pleistocene, J. Paleolimnol., 37(1), 135–153, doi:10.1007/s10933-006-9018-5, 2006.

Lunt, D. J., Abe-Ouchi, A., Bakker, P., Berger, A., Braconnot, P., Charbit, S., Fischer, N., Herold, N., Jungclaus, J. H., Khon, V. C., Krebs-Kanzow, U., Langebroek, P. M., Lohmann, G., Nisancioglu, K. H., Otto-Bliesner, B. L., Park, W., Pfeiffer, M., Phipps, S. J., Prange, M., Rachmayani, R., Renssen, H., Rosenbloom, N., Schneider, B., Stone, E. J., Takahashi, K., Wei, W., Yin, Q. and Zhang, Z. S.: A multi-model assessment of last interglacial temperatures, Clim Past, 9(2), 699–717, doi:10.5194/cp-9-699-2013, 2013.

Lüthi, D., Le Floch, M., Bereiter, B., Blunier, T., Barnola, J.-M., Siegenthaler, U., Raynaud, D., Jouzel, J., Fischer, H., Kawamura, K. and Stocker, T. F.: High-resolution carbon dioxide concentration record 650,000–800,000 years before present, Nature, 453(7193), 379–382, doi:10.1038/nature06949, 2008.

McKay, R., Naish, T., Powell, R., Barrett, P., Scherer, R., Talarico, F., Kyle, P., Monien, D., Kuhn, G., Jackolski, C. and Williams, T.: Pleistocene variability of Antarctic Ice Sheet extent in the Ross Embayment, Quat. Sci. Rev., 34, 93–112, doi:10.1016/j.quascirev.2011.12.012, 2012.

Melles, M., Brigham-Grette, J., Minyuk, P. S., Nowaczyk, N. R., Wennrich, V., DeConto, R. M., Anderson, P. M., Andreev, A. A., Coletti, A., Cook, T. L., Haltia-Hovi, E., Kukkonen, M., Lozhkin, A. V., Rosen, P., Tarasov, P., Vogel, H. and Wagner, B.: 2.8 Million Years of Arctic Climate Change from Lake El'gygytgyn, NE Russia, Science, 337(6092), 315–320, doi:10.1126/science.1222135, 2012.

Miller, G. H., Alley, R. B., Brigham-Grette, J., Fitzpatrick, J. J., Polyak, L., Serreze, M. C. and White, J. W. C.: Arctic amplification: can the past constrain the future?, Quat. Sci. Rev., 29(15-16), 1779–1790, doi:10.1016/j.quascirev.2010.02.008, 2010a.

Miller, G. H., Brigham-Grette, J., Alley, R. B., Anderson, L., Bauch, H. A., Douglas, M. S. V., Edwards, M. E., Elias, S. A., Finney, B. P., Fitzpatrick, J. J., Funder, S. V., Herbert, T. D., Hinzman, L. D., Kaufman, D. S., MacDonald, G. M., Polyak, L., Robock, A., Serreze, M. C., Smol, J. P., Spielhagen, R., White, J. W. C., Wolfe, A. P. and Wolff, E. W.: Temperature and precipitation history of the Arctic, Spec. Theme Arct. Palaeoclim. Synth. PP 1674-1790, 29(15–16), 1679–1715, doi:10.1016/j.quascirev.2010.03.001, 2010b.

Nolan, M. and Brigham-Grette, J.: Basic hydrology, limnology, and meteorology of modern Lake El'gygytgyn, Siberia, J. Paleolimnol., 37(1), 17–35, doi:10.1007/s10933-006-9020-y, 2006.

574 Otto-Bliesner, B. L., Marshall, S. J., Overpeck, J. T., Miller, G. H., Hu, A. and CAPE
575 Last Interglacial Project Members: Simulating Arctic Climate Warmth and Icefield
576 Retreat in the Last Interglaciation, Science, 311(5768), 1751–1753,
577 doi:10.1126/science.1120808, 2006.

578 Pollard, D. and DeConto, R. M.: Modelling West Antarctic ice sheet growth and collapse
579 through the past five million years, Nature, 458(7236), 329–332,
580 doi:10.1038/nature07809, 2009.

581 Polyak, L., Alley, R. B., Andrews, J. T., Brigham-Grette, J., Cronin, T. M., Darby, D. A.,
582 Dyke, A. S., Fitzpatrick, J. J., Funder, S., Holland, M., Jennings, A. E., Miller, G. H.,
583 O'Regan, M., Savelle, J., Serreze, M., St. John, K., White, J. W. C. and Wolff, E.:
584 History of sea ice in the Arctic, Spec. Theme Arct. Palaeoclim. Synth. PP 1674-1790,
585 29(15–16), 1757–1778, doi:10.1016/j.quascirev.2010.02.010, 2010.

586 Prokopenko, A. A., Bezrukova, E. V., Khursevich, G. K., Solotchina, E. P., Kuzmin, M.
587 I. and Tarasov, P. E.: Climate in Continental Interior Asia During the Longest Interglacial
588 of the Past 500000 Years: The New MIS 11 Records from Lake Baikal, SE Siberia, Clim
589 Past, 6, 31–48, 2010.

590 Quiquet, A., Ritz, C., Punge, H. J. and Salas y Mélia, D.: Greenland ice sheet
591 contribution to sea level rise during the last interglacial period: a modelling study driven
592 and constrained by ice core data, Clim Past, 9(1), 353–366, doi:10.5194/cp-9-353-2013,
593 2013.

594 Raymo, M. E. and Mitrovica, J. X.: Collapse of polar ice sheets during the stage 11
595 interglacial, Nature, 483(7390), 453–456, doi:10.1038/nature10891, 2012.

596 Robinson, A., Calov, R. and Ganopolski, A.: Greenland ice sheet model parameters
597 constrained using simulations of the Eemian Interglacial, Clim Past, 7(2), 381–396,
598 doi:10.5194/cp-7-381-2011, 2011.

599 Scherer, R. P., Bohaty, S. M., Dunbar, R. B., Esper, O., Flores, J.-A., Gersonde, R.,
600 Harwood, D. M., Roberts, A. P. and Taviani, M.: Antarctic records of precession-paced
601 insolation-driven warming during early Pleistocene Marine Isotope Stage 31, Geophys.
602 Res. Lett., 35(3), doi:10.1029/2007GL032254, 2008.

603 Schilt, A., Baumgartner, M., Blunier, T., Schwander, J., Spahni, R., Fischer, H. and
604 Stocker, T. F.: Glacial–interglacial and millennial-scale variations in the atmospheric
605 nitrous oxide concentration during the last 800,000 years, Quat. Sci. Rev., 29(1-2), 182–
606 192, doi:10.1016/j.quascirev.2009.03.011, 2010.

607 Serreze, M. C. and Hurst, C. M.: Representation of Mean Arctic Precipitation from
608 NCEP–NCAR and ERA Reanalyses, J. Clim., 13(1), 182–201, doi:10.1175/1520-
609 0442(2000)013<0182:ROMAPF>2.0.CO;2, 2000.

610 Stocker, T. F., Qin, D., Plattner, G.-K., Tignor, M., Allen, S. K., Boschung, J., Nauels,
611 A., Xia, Y., Bex, V. and Midgley (eds.), P. .: IPCC,2013: Climate Change 2013: The

Physical Science Basis. Contribution of Working Group I to the Fifth Assessment Report of the Intergovernmental Panel on Climate Change, Camb. Univ. Press Camb. UK N. Y. NY USA, 1535 pp, doi:10.1017/CBO9781107415324, 2013.

Stone, E. J., Lunt, D. J., Annan, J. D. and Hargreaves, J. C.: Quantification of the Greenland ice sheet contribution to Last Interglacial sea level rise, Clim Past, 9(2), 621–639, doi:10.5194/cp-9-621-2013, 2013.

Tarasov, P. E., Nakagawa, T., Demske, D., Österle, H., Igarashi, Y., Kitagawa, J., Mokhova, L., Bazarova, V., Okuda, M., Gotanda, K., Miyoshi, N., Fujiki, T., Takemura, K., Yonenobu, H. and Fleck, A.: Progress in the reconstruction of Quaternary climate dynamics in the Northwest Pacific: A new modern analogue reference dataset and its application to the 430-kyr pollen record from Lake Biwa, Earth-Sci. Rev., 108(1-2), 64–79, doi:10.1016/j.earscirev.2011.06.002, 2011.

Thompson, S. L. and Pollard, D.: Greenland and Antarctic mass balances for present and doubled atmospheric CO2 from the GENESIS version-2 global climate model, J. Clim., 10(5), 871–900, 1997.

De Vernal, A. and Hillaire-Marcel, C.: Natural Variability of Greenland Climate, Vegetation, and Ice Volume During the Past Million Years, Science, 320(5883), 1622–1625, doi:10.1126/science.1153929, 2008.

Viereck, L. A. and Little Jr, E. L.: Atlas of United States Trees, Volume 2: Alaska Trees and Common Shrubs., 1975.

Willerslev, E., Cappellini, E., Boomsma, W., Nielsen, R., Hebsgaard, M. B., Brand, T. B., Hofreiter, M., Bunce, M., Poinar, H. N., Dahl-Jensen, D., Johnsen, S., Steffensen, J. P., Bennike, O., Schwenninger, J.-L., Nathan, R., Armitage, S., de Hoog, C.-J., Alfimov, V., Christl, M., Beer, J., Muscheler, R., Barker, J., Sharp, M., Penkman, K. E. H., Haile, J., Taberlet, P., Gilbert, M. T. P., Casoli, A., Campani, E. and Collins, M. J.: Ancient Biomolecules from Deep Ice Cores Reveal a Forested Southern Greenland, Science, 317(5834), 111–114, doi:10.1126/science.1141758, 2007.

Woodgate, R. A., Weingartner, T. and Lindsay, R.: The 2007 Bering Strait oceanic heat flux and anomalous Arctic sea-ice retreat, Geophys. Res. Lett., 37(1), n/a–n/a, doi:10.1029/2009GL041621, 2010.

Yin, Q. Z. and Berger, A.: Individual contribution of insolation and CO2 to the interglacial climates of the past 800,000 years, Clim. Dyn., 38(3-4), 709–724, doi:10.1007/s00382-011-1013-5, 2011.

Figures:

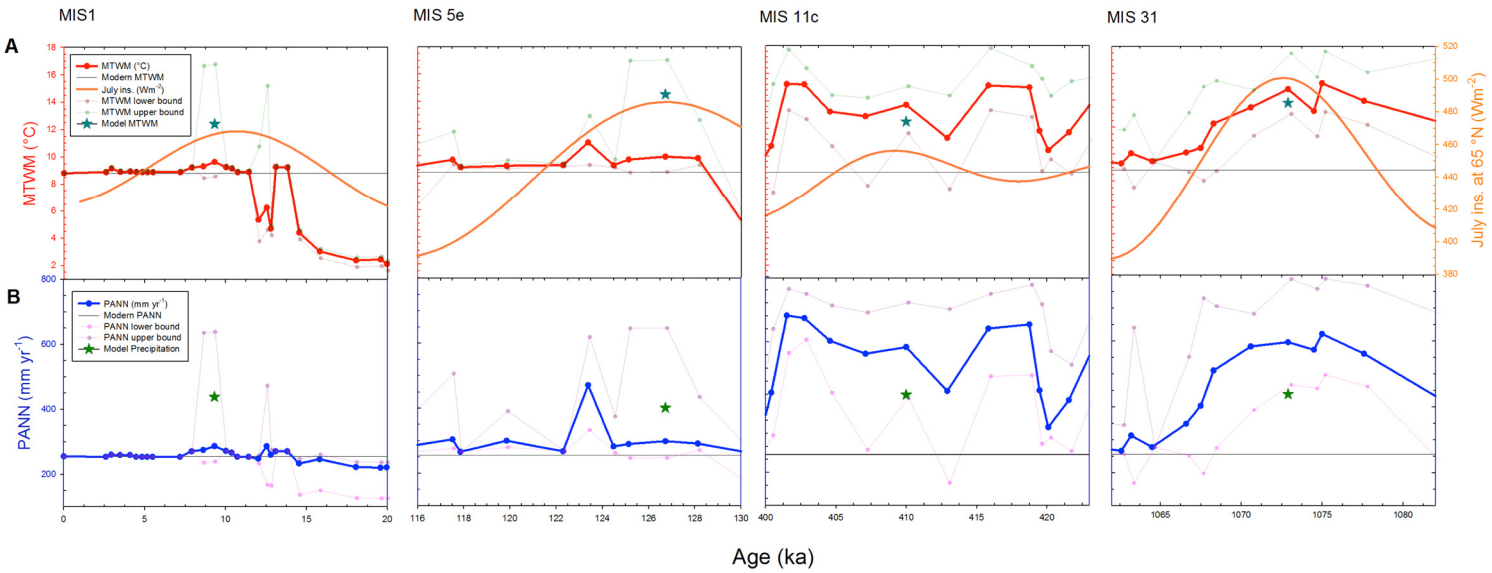

Figure 1: (**A** and **B**) **A** Reconstructed MTWM and **B** PANN from *Melles et al., 2012*. Transparent data above and below the **bolded** lines are upper and lower limits of each data point calculated from a best modern analogue technique (MAT) function. The dark cyan (**A**) and dark green (**B**) stars denote results from the GCM simulations with respect to MTWM and PANN.

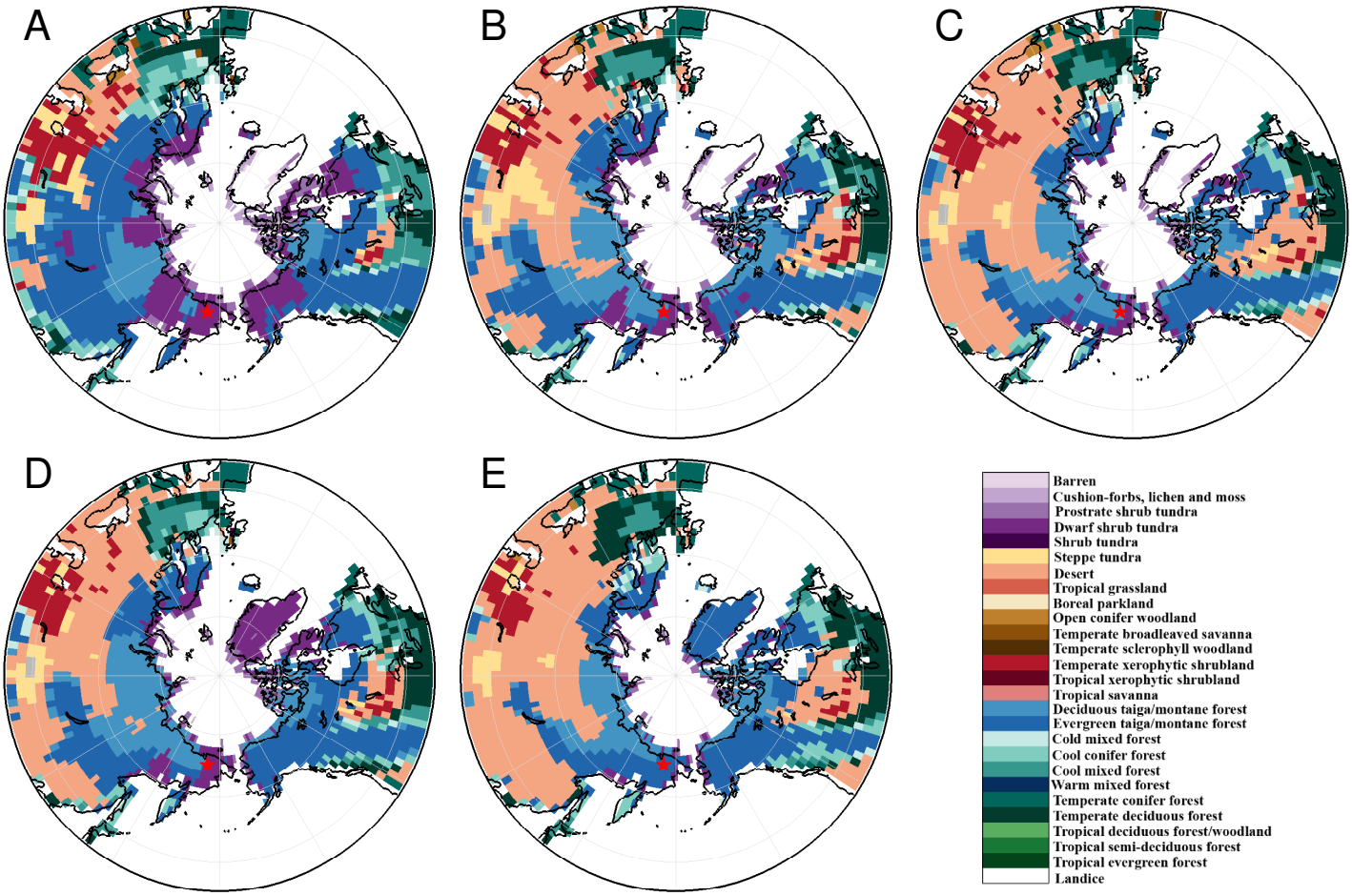

Figure 2: Distribution of interglacial vegetation simulated by the BIOME4 interactive vegetation model coupled to the GCM. A Preindustrial vegetation corresponding to a modern orbit, **B** MIS-1 (9 ka), **C** MIS-5e vegetation, **D** MIS11NG vegetation and **E** MIS-31 (no GIS) vegetation. The location of Lake E is shown near the bottom of each figure with a red star. Note the poleward advancement of evergreen and needle-leaf trees around the lake during each interglacial and the replacement of shrub tundra to taiga forest. *(vegetation data from Melles et al., 2012).*

669
670
671
672
673
674
675
676
677
678
679

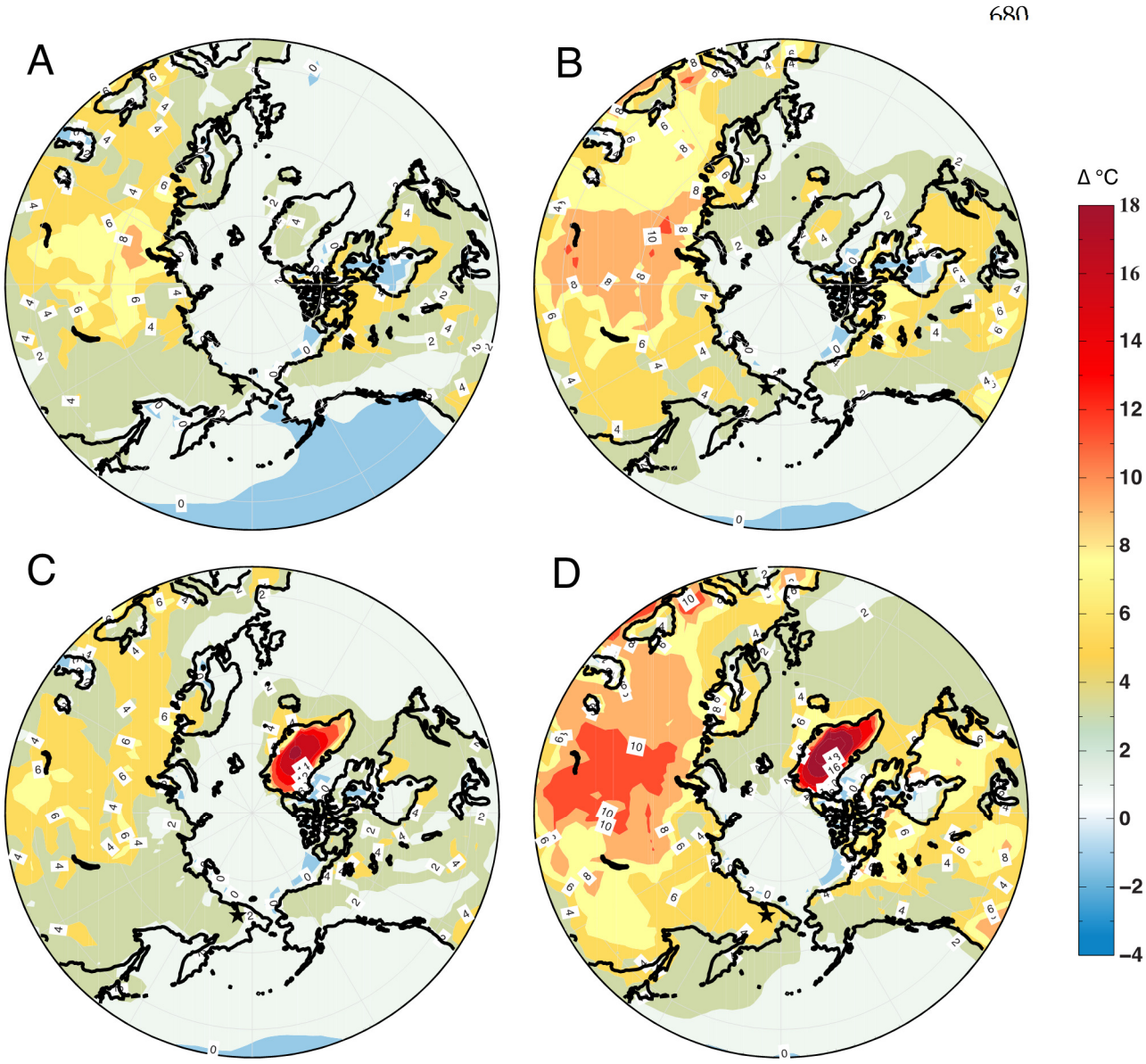

Figure 3: Simulated interglacial anomalies (2-meter annual air temperature in °C) relative to preindustrial temperatures. A MIS-1 (9 ka orbit and GHGs), **B** MIS-5e (127 ka orbit and GHGs), **C** MIS-11c (409 ka orbit and GHGs, and no Greenland Ice Sheet), **D** MIS-31 (1072 ka orbit and GHGs, and no Greenland Ice Sheet). The location of Lake El'gygytgyn (black star) is shown near the bottom of each panel. Areas of no shading (white) roughly correspond to no change that is statistically significant at the 95% confidence interval.

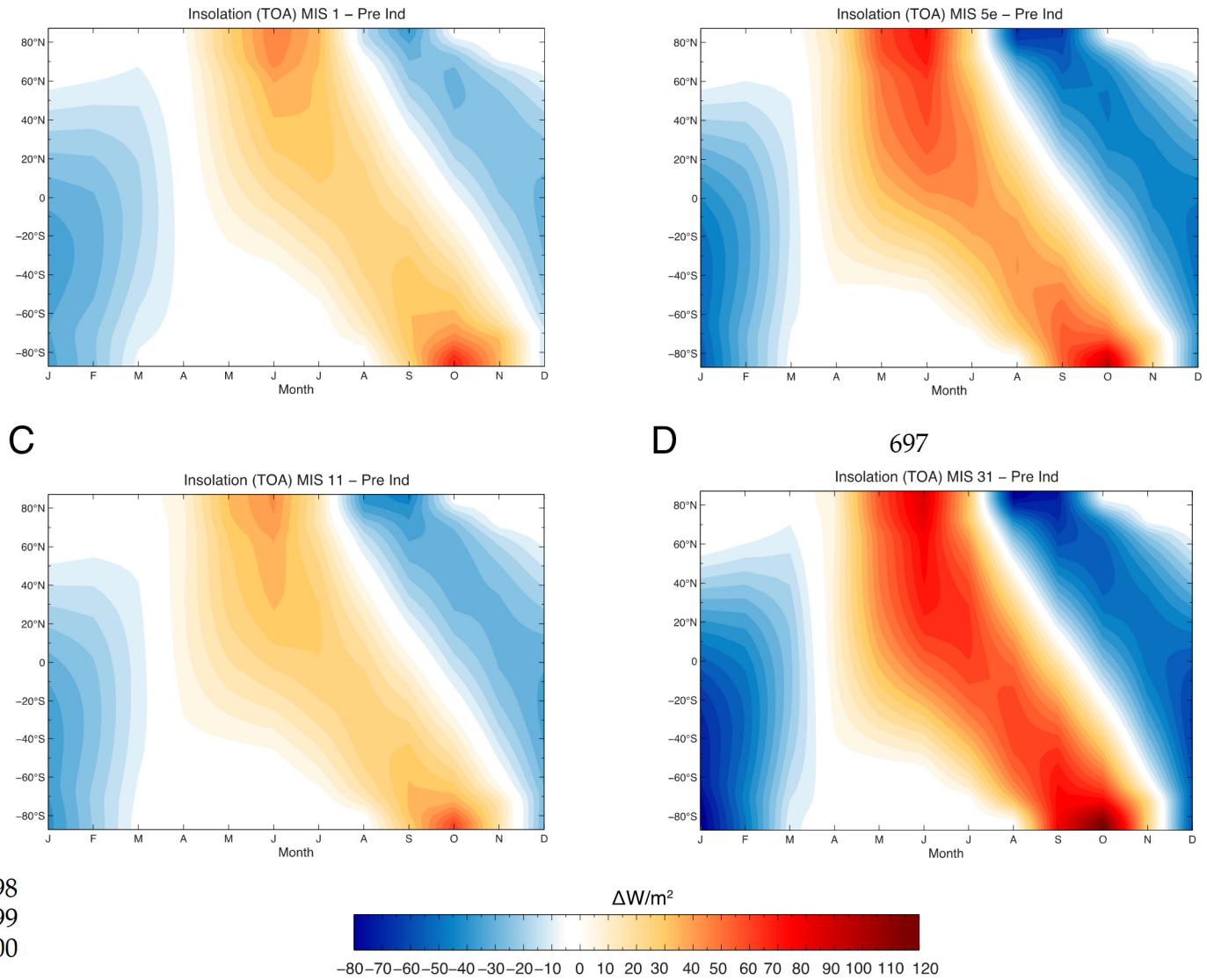

Figure 4: Monthly insolation anomalies at the top of the atmosphere for the interglacial intervals modeled here [W/m^2]. A MIS-1 anomalies with respect to preindustrial (modern) orbit, **B** MIS-5e anomalies with respect to modern orbit, **C** MIS-11c anomalies with respect to modern orbit and **D** MIS-31 anomalies with respect to modern orbit.

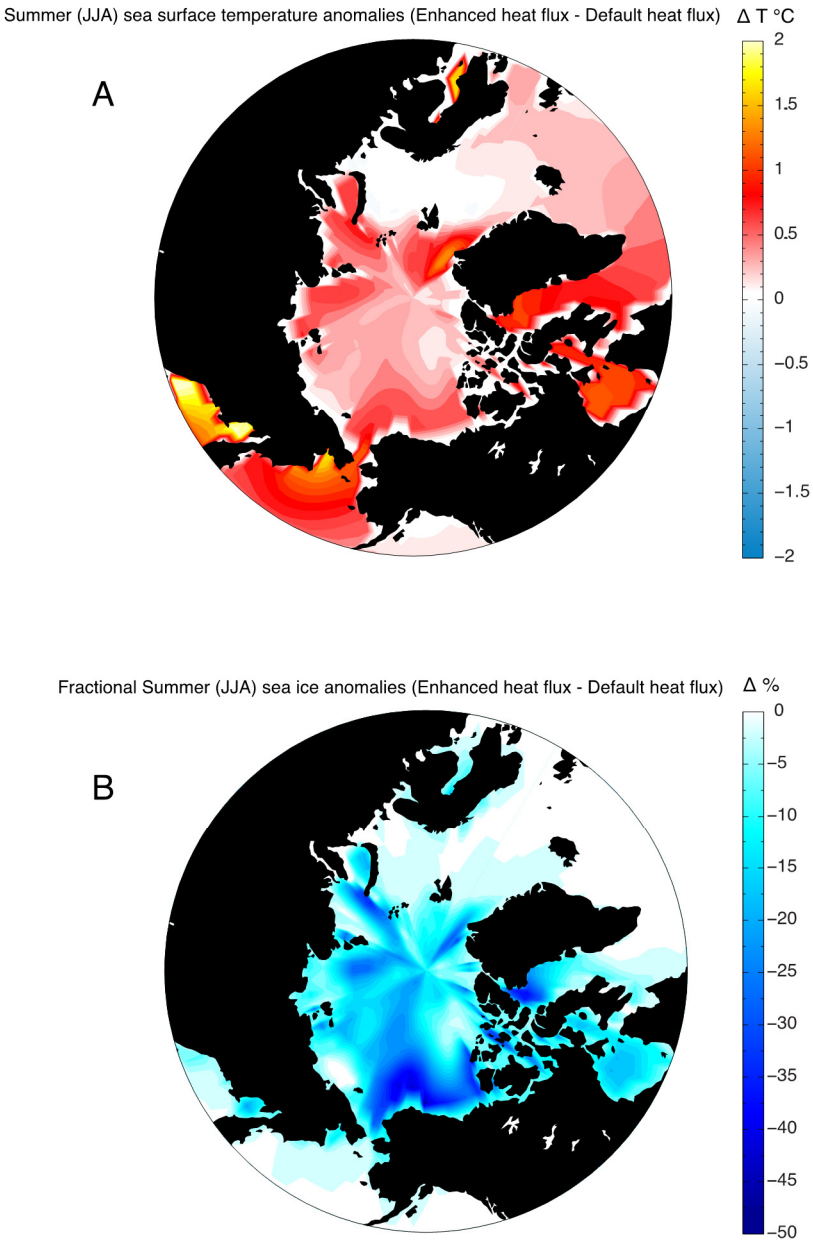

Figure 5: Model simulated (MIS11NG) Summer sea surface temperature and sea ice anomalies caused by enhanced oceanic heat flux (+8 W/m^2) at 409 ka. A Summer (JJA) sea surface temperature change with respect to default heat flux simulation (T °C) and **B** Summer (JJA) sea ice fraction anomalies (%) with respect to default heat flux simulation. With +8 W/m^2 of sub-sea ice heat flux convergence, Arctic Ocean SSTs rise > 0.5 °C and sea ice fraction decreases 25-50% in most areas.

Table 1: Overview of interglacial simulations performed during this study. Orbital configurations **(Berger, 1978)** and greenhouse gas (GHG) concentrations **(Honisch et al., 2009; Loulergue et al., 2008; Lüthi et al., 2008; Schilt et al., 2010)**. Modern GHG concentrations are taken from 1950 AD; obliquity is given in degrees and precession (Ω) in degrees.

Age	Run description	CO_2 (ppmv)	CH_4 (ppbv)	N_2O (ppbv)	Eccentricity	Obliquity (°)	Precession (Ω, °)
1850 AD	pre-industrial simulation with pre-industrial GHG concentrations	280	801	289	0.01671	23.438	101.37
9 ka	MIS 1 - with (modern) GIS	~260	~611	~263	0.01920	24.229	310.32
127 ka	MIS 5e - with (modern) GIS	287	724	262	0.03938	24.040	272.92
409 ka	MIS 11c - with (modern) GIS	285	713	285	0.01932	23.781	265.34
409 ka	MIS 11c - no GIS	285	713	285	0.01932	23.781	265.34
409 ka	MIS 11c - no GIS + 10 Wm^{-2} increase of heat flux under sea ice	285	713	285	0.01932	23.781	265.34
1072 ka	MIS 31 - with no GIS	325	800	288	0.05597	23.898	289.79

790
791
792
793
794
795
796
797

Table 2: List of GCM simulations with corresponding variables at the grid cell location of Lake E. Mean Annual Air Temperature (MAAT), Summer temperature (JJA), Mean Temperature of the Warmest Month (MTWM; July) and Mean Annual Precipitation (PANN) are listed below.

Run	Pre-industrial	MIS 1-with GIS	MIS 5e-with GIS	MIS 11c-with GIS	MIS 11c-no GIS	MIS 11c-noGIS-10Wm^{-2}	MIS 31-without GIS
Lake-E							
MAAT (°C)	-12	-12	-12.4	-11.5	-12.5	-10.5	-10.4
Summer Temp (JJA; °C)	8	9.6	10.5	10	10.2	10.5	11.8
MTWM (July,°C)	10.3	12.4	14.5	12.2	12.5	13.2	13.8
PANN (mm yr^{-1})	438	438	401	475	438	475	438